JET MOTION, INTERNAL WORKING SURFACES, AND NESTED SHELLS IN THE PROTOSTELLAR SYSTEM HH 212

Chin-Fei Lee, Naomi Hirano, Qizhou Zhang, Hsien Shang, Paul T.P. Ho, and Yosuke Mizuno

Accepted by ApJ http://arxiv.org/pdf/1503.07362

Intro.

- Protostellar Jetは星形成の質量降着プロセスに密接に関係し重要
  超音速でコリメートしており、曲がった構造やノットやbow shockが見られる。

- HH212
  - Orion分子雲のL1630にあるClass0原始星IRAS05413-0104（距離 d ~ 400pc、L~9$L_\odot$）が放出源
  - ほとんど天球面方向（<5deg)のコリメートしたジェット
  - もっともよく調べられている原始星ジェットの１つで、H2振動励起も観測されている。
  - Lee+2008で、SiOにより回転運動が観測されている（~0.35”分解能）
    ※0.5”での確認が必要

Observation

- ALMA Cycle0 (2012年12月観測)
- SiO (J = 8−7) and CO (J = 3−2)を9-pointing mosaic (中心星から±40” の領域をmapping)
- 7.7 mJy/beam (i.e., 0.32 K), Beam 0".53×0".47

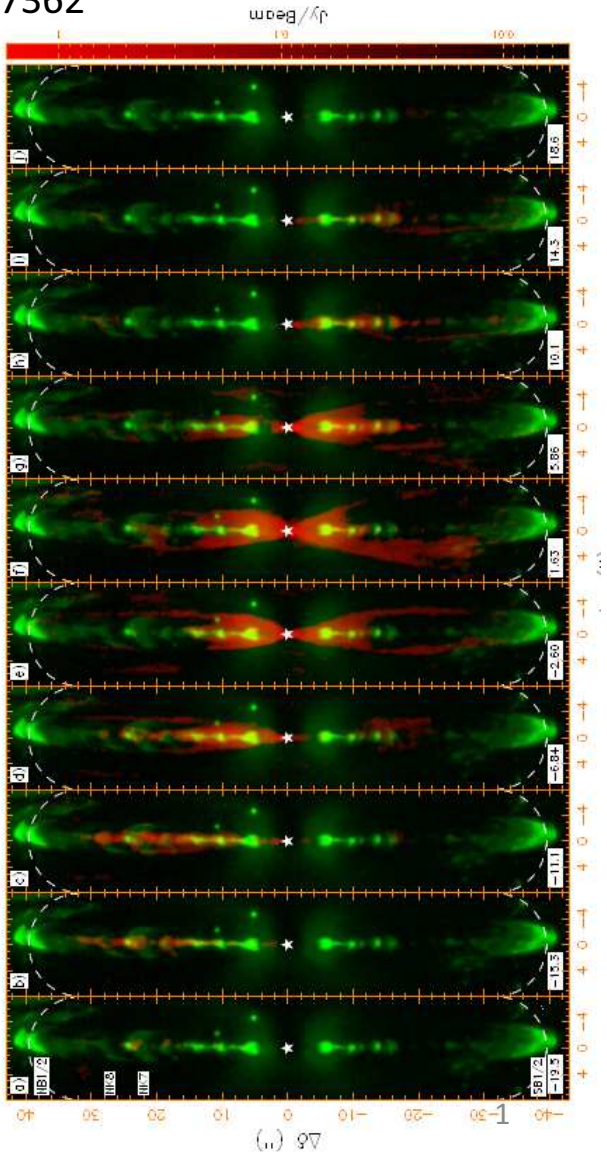

⇒
Fig1. COのchannle map（赤）+ リファレンスのH2振動励起image (緑)。
COのコーンの広がりは外側の巨大Bow Shockにつながっている。
Cavity Wall?

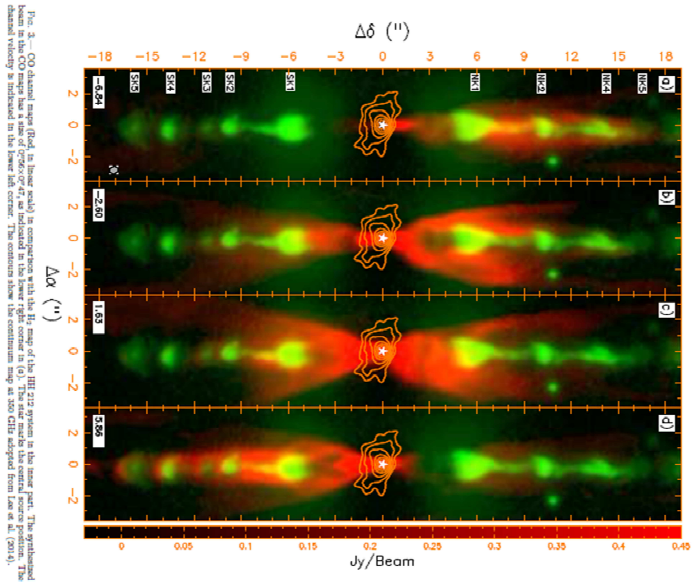

Fig3　中心領域拡大。たくさんのInternal Shellがあり、CO emisionがそれを取り巻いている（see Lee+2007）。
Fig3 d) v=5.86km/sで、jet軸に沿って南側にヘリカル構造がある。

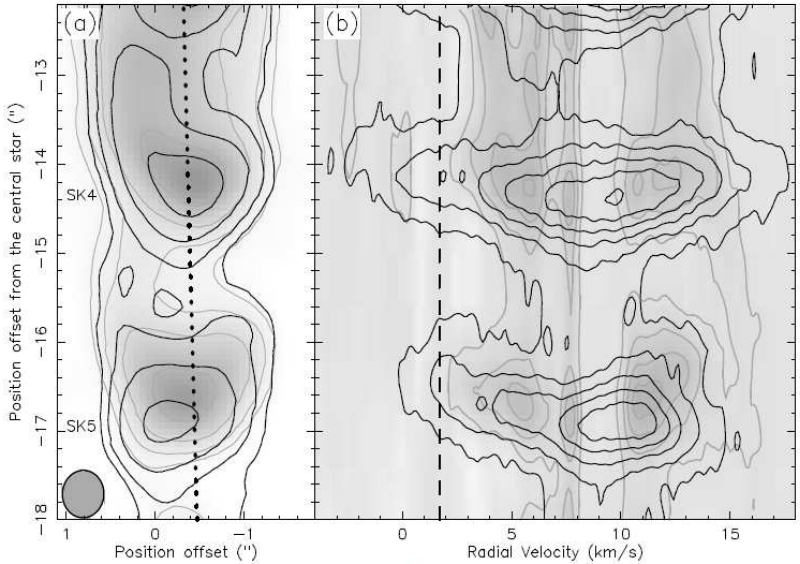

FIG. 6.— Structure and kinematics of knots SK4 and SK5 in the south. Gray contours with image are for CO and black contours are for SiO. (*a*) The SiO map is the same as in Figure 4 but zooming into knots SK4 and SK5, highlighting their bowlike structures. The CO map shows the total CO emission of knots SK4 and SK5 integrated from 2.2 to 15.4 km s^{-1}. Contour levels are $0.25 \times 2^{n-1}$ Jy $beam^{-1}$ km s^{-1}, where $n = 1, 2, 3...$ The dotted line indicates the jet axis in the south. (*b*) Position-velocity (PV) diagrams cut along the jet axis for knots SK4 and SK5. The vertical dashed line indicates the systemic velocity of 1.7 km s^{-1}. The contour levels start at 40 mJy $beam^{-1}$ with a step of 160 mJy $beam^{-1}$ for CO, and start at 30 mJy $beam^{-1}$ with a step of 120 mJy $beam^{-1}$ for SiO.

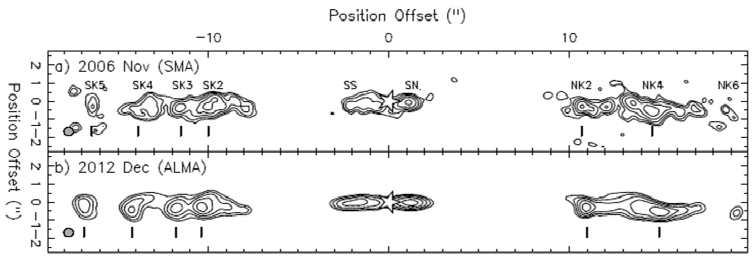

Fig5. 6年前のSMA観測とALMAのSiOの位置比較。
固有運動は0.06" per year ⇔ 115±50km/s (tangential velocity)。これは1.1x10^{-6}M$_{\odot}$/yrに相当（降着の20%)

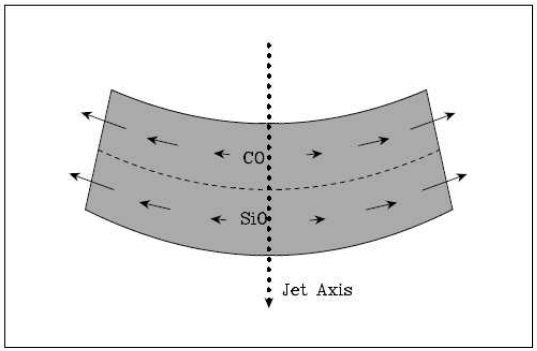

FIG. 7.— Velocity structure of the shocked material in an internal working surface (IWS) in the shock frame moving down the jet axis. The vectors show the material motion, with the length showing the magnitude. Two layers, CO and SiO, are plotted as an illustration based on our observational results.

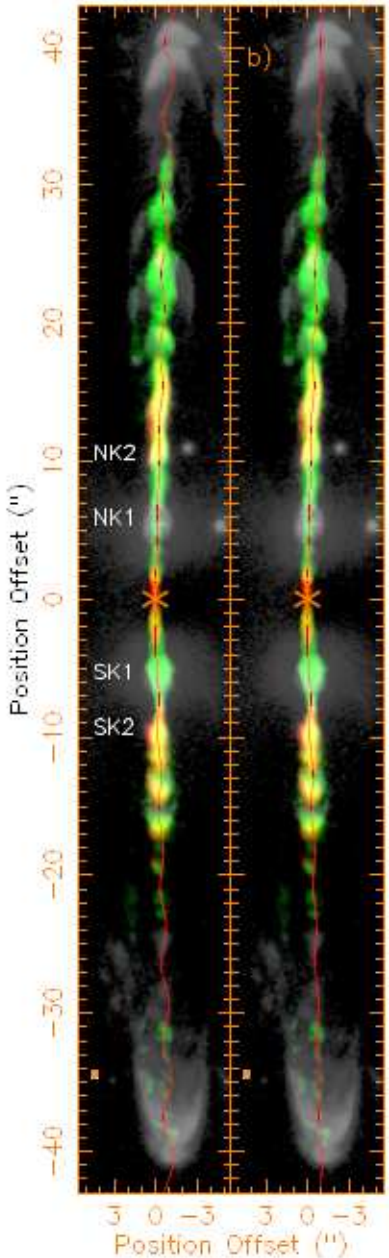

- 歳差運動？ヘリカル磁場？
- Wiggleは5.6"の波長 ⇔ 歳差なら 93年周期
- 振幅の成長をを10"以遠でなしとすると観測と合う(b)
  ただし、どう解釈していいのかは謎

Fig8 jetのwiggle。
H2振動励起 (Gray) + High Velocity CO (Green) + SiO (Red)
赤い線はモデル
a) 中心からの距離に比例して振幅が増加
b) 10"以遠では同じ振幅

FIG. 8.— The wiggle of the jet and the model (red curves) for the wiggle. Gray image is H_2, green image is high-velocity CO, and red image is SiO from Figure 4. (a) The model assumes a constant growth in the wiggle amplitude with the distance from the central source. (b) A revised model assumes a constant wiggle amplitude for a distance greater than 10″ from the central source.

X-ray emission from stellar jets by collision against high-density molecular clouds: an application to HH 248

J. Lo'pez-Santiago, R. Bonito, M. Orellana, M. Miceli, S. Orlando, S. Ustamujic, J.F. Albacete-Colombo, E. de Castro, A.I. Go'mez de Castro

Accepted by ApJ http://arxiv.org/pdf/1503.03717

Intro.

- Stellar jetによる衝撃波は電波～紫外線で波長で観測されている。
- HH jetにX-rayが付随することがPravdo+(2001)により報告(HH 2)。
  以後も数多くの報告：HH154 from L1551IRS5, HH80/81, HH540,,,)。
- HH jetに付随するX-rayは2つのタイプ（Bonito+2010b)
  - 星から2000AU以内の高温emission (T>2x10^{6}K)
  - 数1000AU以遠の低温emission(広がっているluminosityは大）。

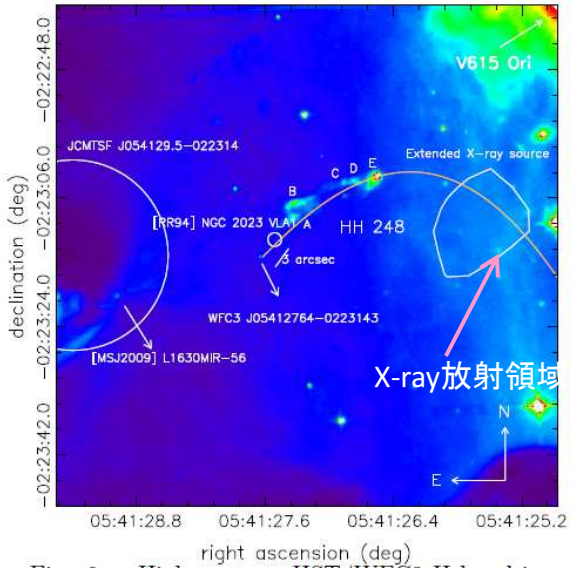

Fig6 HH248（橙の実線）領域の HST/WFC3 H Bandイメージ。
WFC3 J05412764-0223243が励起星？

Model・Caluculation

- FLASH codeを用いた数値シミュレーション
- 軸対称 2D Cylindrical coordinate (r, z)
- r = 1400AU x z = 14000AUの計算領域
  （実効的に~7AU分解能で128x1280grid)
- 光学的に薄いプラズマからの放射冷却、、、、
- モデル設定とパラメータ (see Fig1):
  - ISMとjetの密度比、
  - wallとjetの密度比、
  - jetの速度 (jet温度は10,000Kで固定）

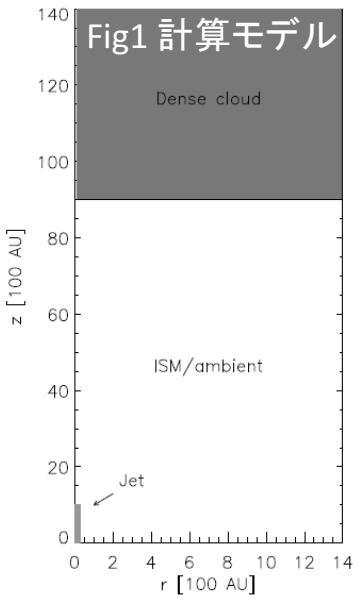

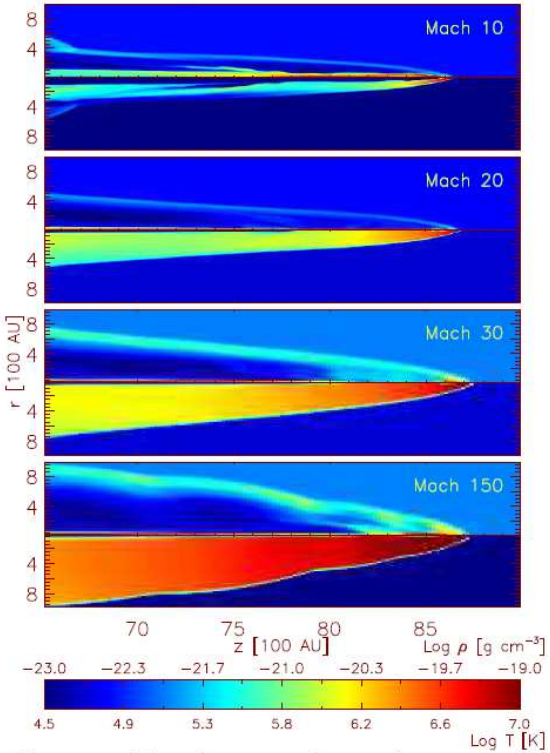

Fig. 3.— Two-dimensional mass density (upper half-panels) and temperature (lower half-panels) cuts in the r–z plane when the jet reaches 8000 AU from the beginning of the simulation. All the simulations are for $n_{\rm ambient}/n_{\rm jet} = 0.1$ but different Mach numbers.

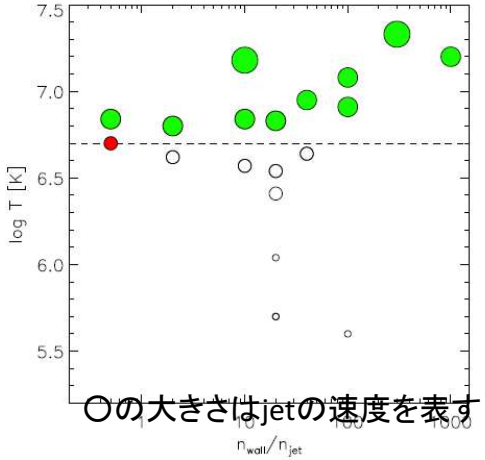

〇の大きさはjetの速度を表す

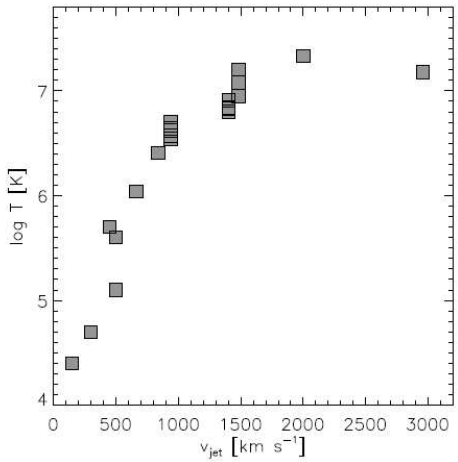

Fig. 4.— **Top:** Maximum temperature of the jet after impacting the dense cloud for the different simulations, compared to the ratio between the jet and the dense cloud densities. Circle sizes are as in Figure 2. The dashed line indicates a temperature of 5 MK ($kT = 0.43$ keV). Filled circles are cases in which the jet reaches temperatures consistent with detected jets in X-rays. **Bottom:** Temperature distribution as a function of the velocity of the jet.

⇒ 700km/sを超えるとx-ray放射密度比への依存性は小さい

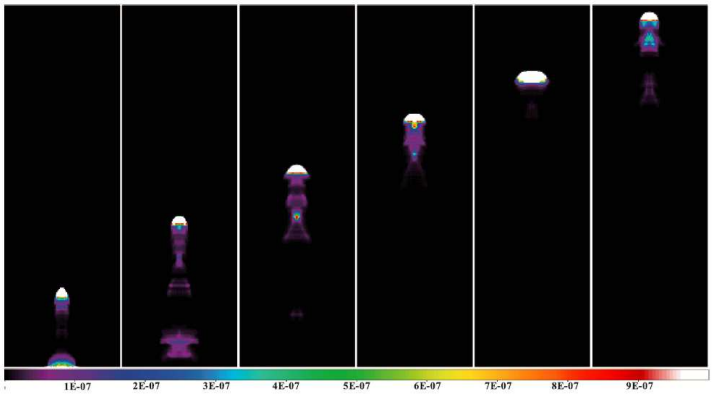

Fig. 8.— X-ray map of the jet after it reaches the high-density molecular cloud (*wall*). The period range is 40–65 yr with a time binning of 5 yr. The pixel size if 1 AU. The color scale is 10^{-7}–10^{-6} cnt s^{-1} pixel^{-1}.

Fig.8 X線の強度分布（jet がwall突入後の時間進化）

シミュレーションで得られた$L_{\rm x\text{-}ray}$ ~ 10^{31} erg/s (Intrinsic)は、HH248の$L_{\rm x\text{-}ray}$ ~ 3×10^{30} erg/s を説明できる。
同様に、シミュレーションで得られたEM～10^{53} cm^{-3}はHH248のEM~2×10^{53} cm^{-3}と一致。

↓

HH jetから観測されているX-rayは、HH jetとdense gasとの衝突で放射されているというシナリオは物理的にあり得る。

Initial Fragmentation in the Infrared Dark Cloud G28.53-0.25

Xing Lu, Qizhou Zhang, Ke Wang and Qiusheng Gu

Accepted by ApJ http://arxiv.org/pdf/1503.08797

Intro.

- Infrared Dark Clouds (IRDCs)は大質量形成をしている母体。
  - < 0.1 pcスケールに分裂していき、それが大質量星を形成している。
  - 高密度コアは乱流的であり、乱流がサポートや分裂に大きくかかわっているように見える。
- G28.53-0.25
  - 力学距離 d ~ 5.4kpc
  - L ~ 3400$L_\odot$, M_{total} ~$10^4 M_\odot$
  - 10の連続波peak（~数100$M_\odot$）が同定されている(IRAM30m 1.2m連続波）。MM1 ~ MM10
  - MM1が最大質量(~1000$M_\odot$)、MM5は中ぐらいの質量だがMM1より線幅大、MM7/MM8は線幅小

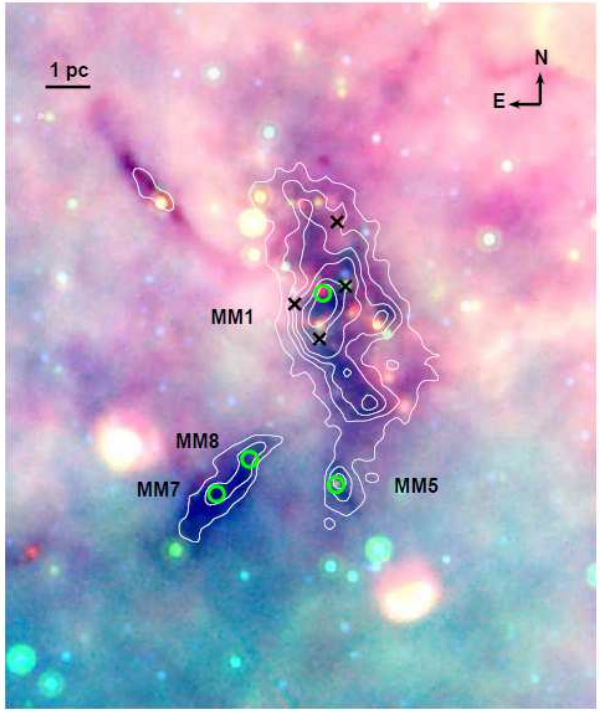

FIG. 1.— *Spitzer* and *Herschel* composite image overlaid with 1.2 mm continuum emission of G28.53 taken from Rathborne et al. (2006). The colors represent emission at 8.0 μm (blue), 24 μm (green), and 70 μm (red) (Churchwell et al. 2009; Carey et al. 2009; Molinari et al. 2010). The contours levels are 30 (3σ), 60, 90, 120, 180, 240 mJy per beam. The four clumps, MM1, MM5, MM7, and MM8 are marked. The green circles mark MM1-p1, MM5-1, MM7-p1, and MM8-p1, the most massive cores in each clump. The four crosses mark the H_2O masers.

Observation

- SMA Compact Config.(2010年PIデータ+Archive)。
  - 230GHz帯 12CO, 13CO, C18O, CH3OH, H2CO
- VLA D-ConfigurationでNH3(1,1), NH3(2,2)を観測

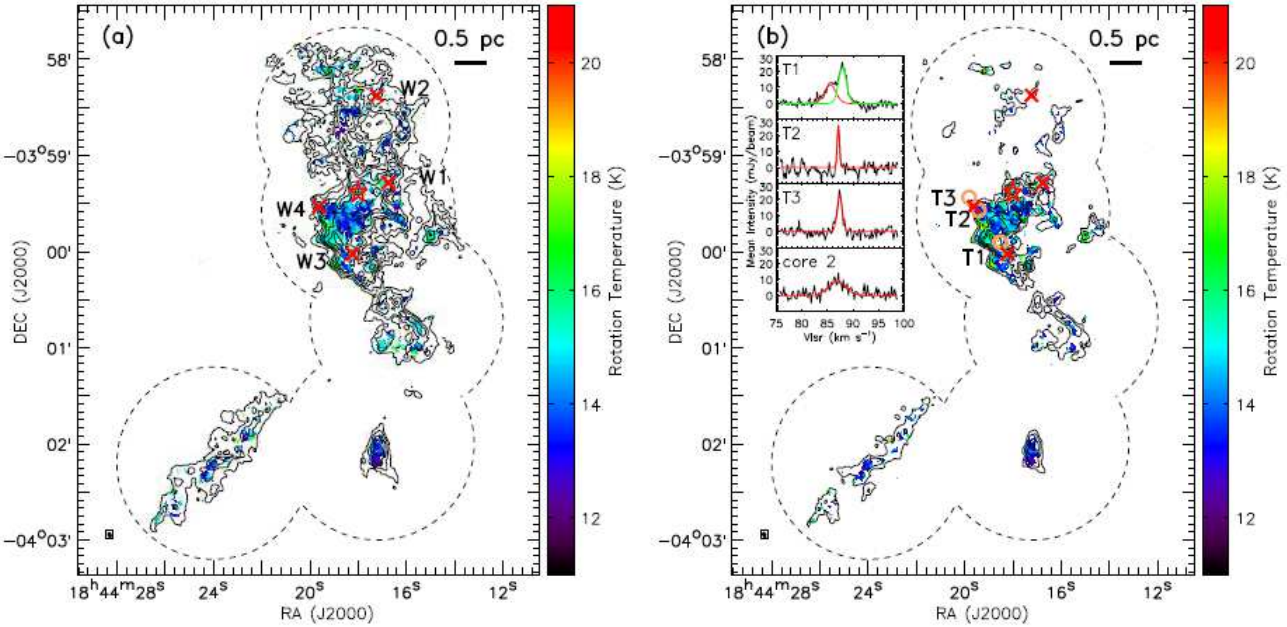

FIG. 2.— NH_3 rotation temperature of G28.53. (a) Temperature map using the combined GBT and VLA data, overlaid with contours of the integrated intensities of the NH_3 (1,1) main hyperfine line. The contours are in steps of 5 mJy beam^{-1} km s^{-1}×[3, 6, 9, 12, 15, 20, 25]. The dash circles represent the 2′ primary beams of the VLA observations. 'Core 2' in MM1 is marked with a star. The four H_2O masers are marked with crosses and labelled as W1–W4. (b) Temperature map using the VLA data only, overlaid with contours of the integrated intensities of the NH_3 (1,1) main hyperfine line. The contours are in steps of 5 mJy beam^{-1} km s^{-1}×[3, 6, 9, 12, 15, 20]. The three positions exhibiting NH_3 (3,3) emission are marked with circles and labelled as T1–T3, with their spectra and the best gaussian fitting shown in the inset. Note that the two maps are plotted using the same color scale from 11 K to 21 K to show their similarity, but the highest temperature in (a) is 19 K.

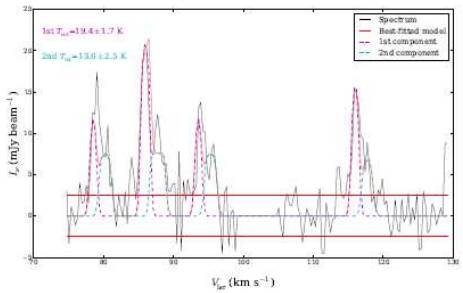

FIG. 4.— Two-components fitting of mean spectra of MM1-p1,

- Fig2. G28.53のNH3 rotation temperature <~17K
- Fig4. MM1は、約2kkm/s離れた2つの速度要素から成る。
  それらの温度は数度ほど異なる。
- (いくつかのcoreに付随するoutflowを発見 ※論文のfig7,8を参照)

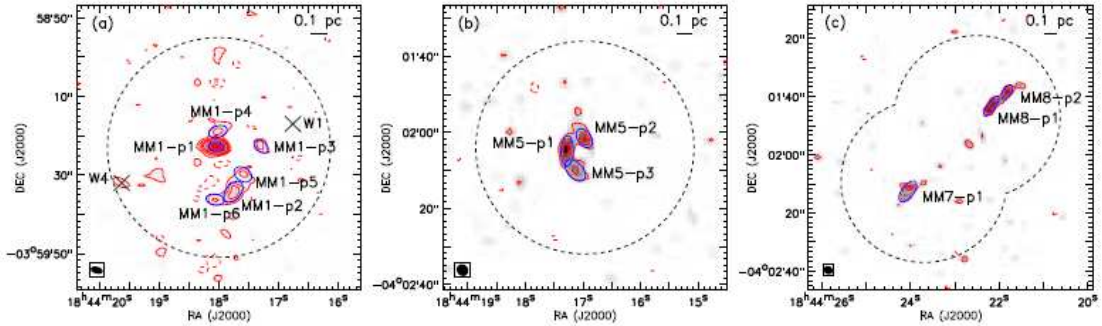

FIG. 5.— The SMA 1.3 mm continuum emission of MM1, MM5 and MM7/8. The dashed circles in each panel mark the 56″ primary beams of the SMA. The ellipses mark FWHM of the 2D gaussians fitted to each core. (a) The contours are in steps of 1.1 mJy beam^{-1}×[−5, −3, 3, 5, 7, 9, 15, 25, 35, 45]. The two H_2O masers, W1 and W4, are marked with crosses. (b) The contours are in steps of 0.9 mJy beam^{-1}×[−3, 3, 5, 7]. (c) The contours are in steps of 0.81 mJy beam^{-1}×[−3, 3, 5, 7].

TABLE 4
CORE PROPERTIES.

Core ID	RA (J2000)	Dec (J2000)	V_{lsr}[a] (km s^{-1})	Maj.×Min.[b] (″×″)	PA[b] (°)	Flux[c] (mJy)	T_{rot} (K)	FWHM (km s^{-1})	M_J[d] ($M_\odot$)		M_{virial}[e] ($M_\odot$)		$M_{virial,\ B=1\,mG}$[f] ($M_\odot$)	M_{core}[g] ($M_\odot$)
MM1-p1	18:44:18.04	−03:59:22.81	87.7	2.2×1.3	103	84.0±3.3	14.0±0.9	1.34	1.9	35.8	5.7	9.5	9.9	56.0±16.5
MM1-p2	18:44:17.76	−03:59:34.31	88.0	5.8×2.2	147	46.8±3.6	13.4±0.4	1.33	1.9	35.8	11.7	19.6	29.5	46.2±13.7
MM1-p3	18:44:17.29	−03:59:22.74	87.8	2.9×1.1	22	15.0±2.1	14.4±0.7	1.31	1.9	35.8	5.8	9.6	13.5	7.3±2.4
MM1-p4	18:44:18.02	−03:59:18.96	87.8	4.0×1.4	124	17.6±0.4	13.6±0.8	1.24	1.9	35.8	6.9	11.5	18.1	13.3±3.9
MM1-p5	18:44:17.60	−03:59:29.85	87.9	3.8×2.7	40	21.0±2.1	13.6±0.5	1.21	1.9	35.8	8.9	14.9	32.1	17.2±5.2
MM1-p6	18:44:18.06	−03:59:36.24	87.8	3.4×2.0	89	16.3±0.2	13.1±0.8	1.26	1.9	35.8	7.8	13.0	20.9	16.4±4.8
MM5-p1	18:44:17.30	−04:02:04.88	87.2	7.3×0.8	177	20.7±2.7	13.6±0.4	1.06	1.4	21.3	5.4	9.0	11.5	38.2±12.0
MM5-p2	18:44:17.01	−04:02:01.54	86.9	4.4×2.0	32	13.5±1.2	13.8±0.4	1.30	1.4	21.3	9.4	15.7	24.6	24.3±7.3
MM5-p3	18:44:17.16	−04:02:10.01	87.0	5.8×2.8	40	14.6±0.1	12.5±0.4	1.12	1.4	21.3	9.7	16.2	40.6	30.4±8.7
MM7-p1	18:44:24.06	−04:02:12.60	88.2	7.9×2.7	144	19.6±4.2	13.7±0.4	1.00	6.0	58.5	9.4	15.6	130.5	11.1±4.0
MM8-p1	18:44:22.18	−04:01:43.30	88.1	<8.0×2.7	···	18.5±1.4	13.5±0.5	1.05	2.9	37.9	10.2	17.0	69.9	24.7±7.3
MM8-p2	18:44:21.83	−04:01:38.38	88.0	<5.4×2.9	···	14.5±0.8	14.6±0.7	1.23	2.9	37.9	11.5	19.1	58.9	17.3±5.1

[a] V_{lsr} of the cores were determined from cross-correlations between a model and the NH_3 (1,1) spectra. For the cores in MM1 that exhibit two velocity components, the ones at ∼87 km s^{-1} are listed (cf. Table 3).
[b] Major and minor FWHMs and position angles of the cores were deconvolved from beam. For MM8-p1 and MM8-p2 that are not resolved, upper limits of major and minor FWHMs are given.
[c] Fluxes are corrected for primary-beam response. Errors listed here are from 2D gaussian fittings, not including 20% uncertainty in flux calibration of the SMA data.
[d] The two columns list thermal Jeans masses and turbulent Jeans masses of the clumps, respectively.
[e] The two columns list virial masses assuming radial density profile of $\rho \sim r^{-2}$ and constant radial density profile respectively.
[f] The total virial mass assuming constant radial density profile and magnetic field strength B=1 mG.
[g] For the cores in MM1, the masses have been scaled to those of the 87 km s^{-1} component, based on the ratios of NH_3 column densities of the two components listed in Table 3.

$$\alpha = M_{\rm virial}/M_{\rm core}$$

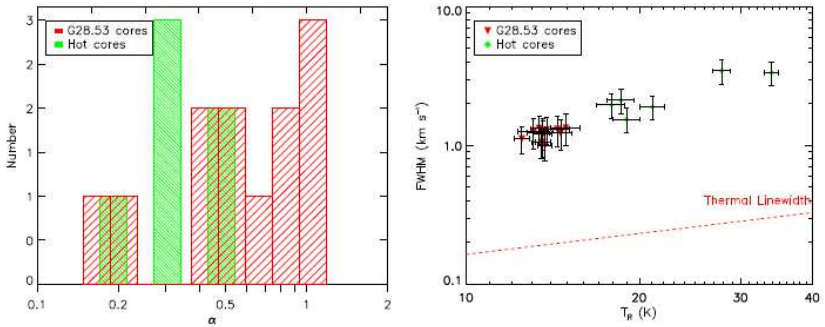

FIG. 9.— *Left*: Virial parameters of cores in G28.53 as well as in the hot core sample of Lu et al. (2014). Constant radial density profiles are assumed for all cores. *Right*: FWHM linewidths vs. rotation temperatures of cores in G28.53 as well as in the hot core sample of Lu et al. (2014).

- 0.1pcのガスの塊は、自己重力不安定状態（α < 1 ）
- 線幅は熱的ではなく、乱流的

Planetary Collisions outside the Solar System: Time Domain Characterization of Extreme Debris Disks

Huan Y. A. Meng, Kate Y. L. Su, George H. Rieke, Wiphu Rujopakarn, Gordon Myers, Michael Cook, Emery Erdelyi, ChrisMaloney, JamesMcMath, Gerald Persha, Saran Poshyachinda, Daniel E. Reichart

Accepted by ApJ http://arxiv.org/pdf/1503.05610

Intro.

- Extreme Debris Disk
  - $f_d = L_{disk}/L_* > \sim 10^{-2}$ ※通常は~10^{-4}
  - 原始惑星の巨大衝突の直後と思われる
  - いくつかのExtreme Debris Diskは1年かそれ以下の時間スーケールでの強度変動がある
  - 中心星が t = 10~200Myr (BD+20 307の1Gyrは例外)

Observation

- Targets
  - $f_d = L_{disk}/L_* > \sim$several x 10^{-3}
  - スペクトル型 = F or mid-K dwarf
  - Silica or Silicate (~9-10micron)のfeature(最近の衝突の指標)
  - 3.6micronと4.5micronのフラックス強度超過が大きい($T_{disk} > \sim 400K$)

  => P1121, HD15407A, HD23514, HD145263, BD+20 307
- Observation&Data
  - 主データ: Spitzer IRAC3.6um, 4.6um観測 + 2MASSSデータ
  - Spitzer 毎年 2回の30-50daysのvisibility window (その間、5日毎の観測)

Fig1

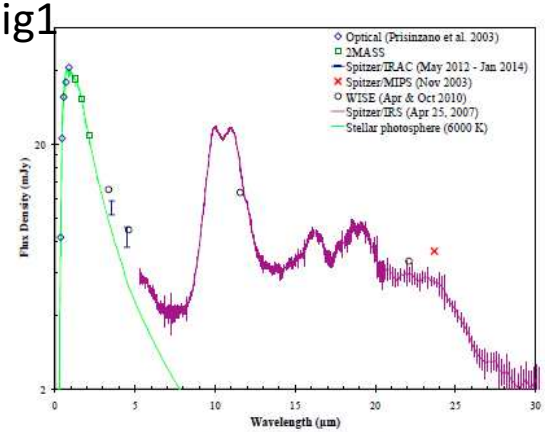

Figure 1. SED of P1121. The vertical bars with caps at 3.6 and 4.5 μm represent the full range of the disk flux observed at each waveband in this work, from 2012 to early 2014.

Fig3 P1121 時間変動の解析

SigSpec algorithm(Reege 2007)の結果図
※ようするにフーリエ解析的なもの

=> ~18dayにpeak (だが統計不足)

Auto-Correlatoin Function

$$ACF(\tau) = \frac{1}{(N-\tau)\sigma_a^2} \sum_{k=1}^{N-\tau} (a_k - \langle a \rangle)(a_{k+\tau} - \langle a \rangle) \quad (4)$$

=> 15day-20dayのmodulation

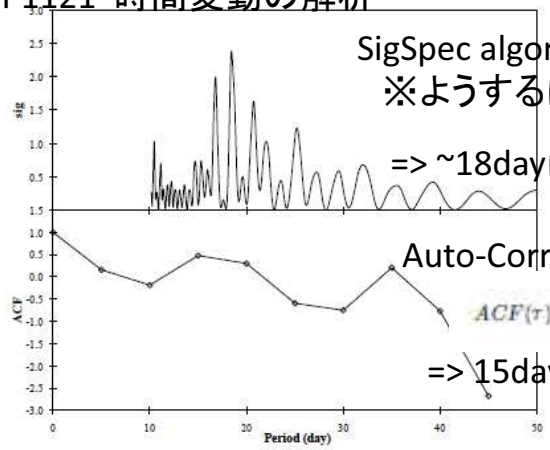

Figure 3. Analysis of the detrended 4.5 μm data of the P1121 disk. Upper: SigSpec periodogram. The strongest signal is at ~18 days with sig = 2.65. Lower: ACF with a time step of 5 days. The first local maximum between 15 and 20 days is the characteristic timescale, corroborated by the second local maximum around 35 days.

Fig2 P1121のflux時間変化

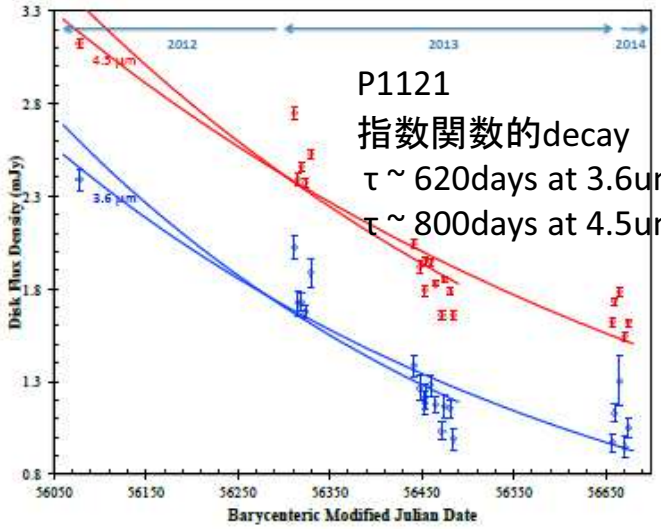

P1121
指数関数的decay
τ ~ 620days at 3.6um
τ ~ 800days at 4.5um

Figure 2. Infrared light curve of the P1121 disk. Overlaid are the fits to the data assuming they follow an exponential decay. The dashed and solid lines represent fit 1 (including all the data) and fit 2 (excluding the 2014 data), respectively.

Fig4 P1121 円盤カラーの時間変化
P1121の[3.6]-[4.5]~7.7 だが星成分を引いたもの

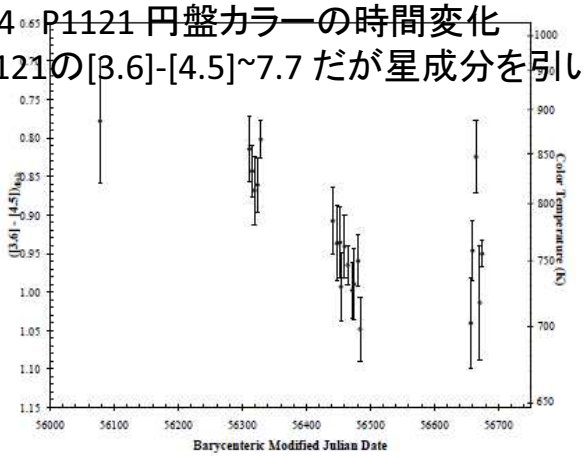

Figure 4. Evolution of the color index and temperature of the P1121 disk.

⇒ 円盤温度が
時間とともに低下。

指数関数的decay(とすると)
τ ~ 1720days at 3.6um
τ ~ 2780days at 4.5um

Fig6 HD15407A

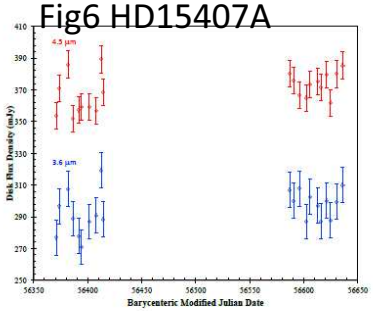

Figure 6. Infrared light curve of the HD 15407A disk in 2013. Synchronous variations between the two wavebands are apparent clear monotonic trend.

Fig8 HD23514

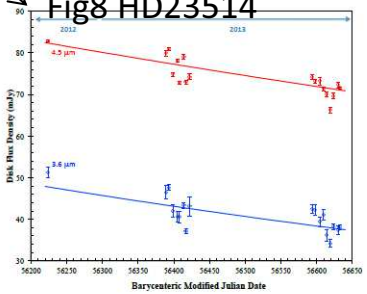

Figure 8. Infrared light curve of the HD 23514A disk. Overlaid lines are the best-fit exponential decay to the data in both wavebands. However, because the fitted timescales are much longer than the time baseline of observations, the assumption of a monotonic decay may be problematic and the fits may be purely phenomenological.

Fig10 HD145263

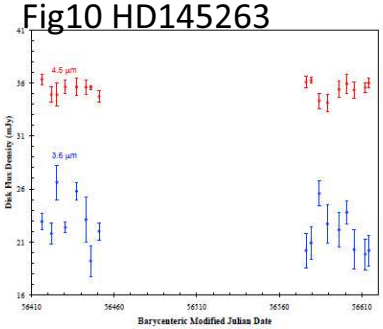

Infrared light curve of the HD 145263 disk in 2013. Analysis reveals no significant variations in 2013.

Fig12 BD+20 307

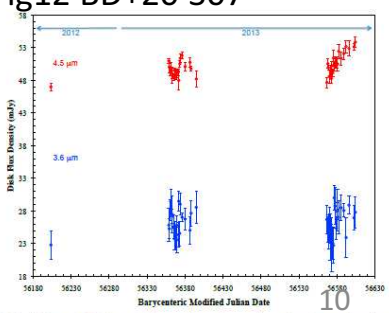

Figure 12. Infrared light curve of the BD+20 307 disk in 2012 and 2013, showing no decay and significant growth trend at 4.5 μm.

Outer Rotation Curve of the Galaxy with VERA II: Annual Parallax and ProperMotion of the Star-Forming Region IRAS21379+5106

Hiroyuki Nakanishi, Nobuyuki Sakai, Tomoharu Kurayama, Mitsuhiro Matsuo, Hiroshi Imai, Ross A. Burns, Takeaki Ozawa, Mareki Honma, Katsunori Shibata, and Noriyuki Kawaguchi

ccepted by PASJ http://arxiv.org/pdf/1503.07273

Intro.

- "Outer Rotation Curve" (ORC) Project
  - VERAのメインプロジェクトの1つ
  - 太陽より外側の銀河回転を調べる。

- IRAS 21379+5106 (Fig1のgreen circle)
  - ultra-compact HII region
  - Perseus armに付随
  - 5.9kpcのkinematic distance (Wang+2009)

Observation

- VERA VLBIで2009年11月～2011年11月に9回観測
- 22.232GHz – 22.248GHzのH2Oメーザー

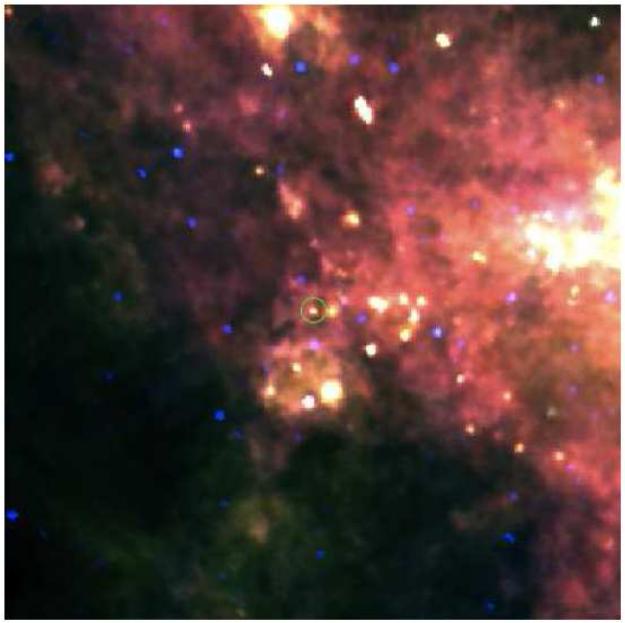

Fig. 1. Mid-Far infrared composite image of $7.^{\circ}5 \times 7.^{\circ}5$ area centered on IRAS 21379+5106. This was made using IRIS 25 μm-, 60 μm-, and 100 μm-band images. IRAS 21379+5106 is indicated with a green circle. A circular-shaped emission region just below IRAS 21379+5106 is the H II region Sharpless 124 (S124). A bright point source located at the southern edge of the circular-shaped infrared emission of S124 is AFGL 2789.

Fig.3 観測されたメーザースポットのoffset
+ annual parallax/liner proper motionのbest fit

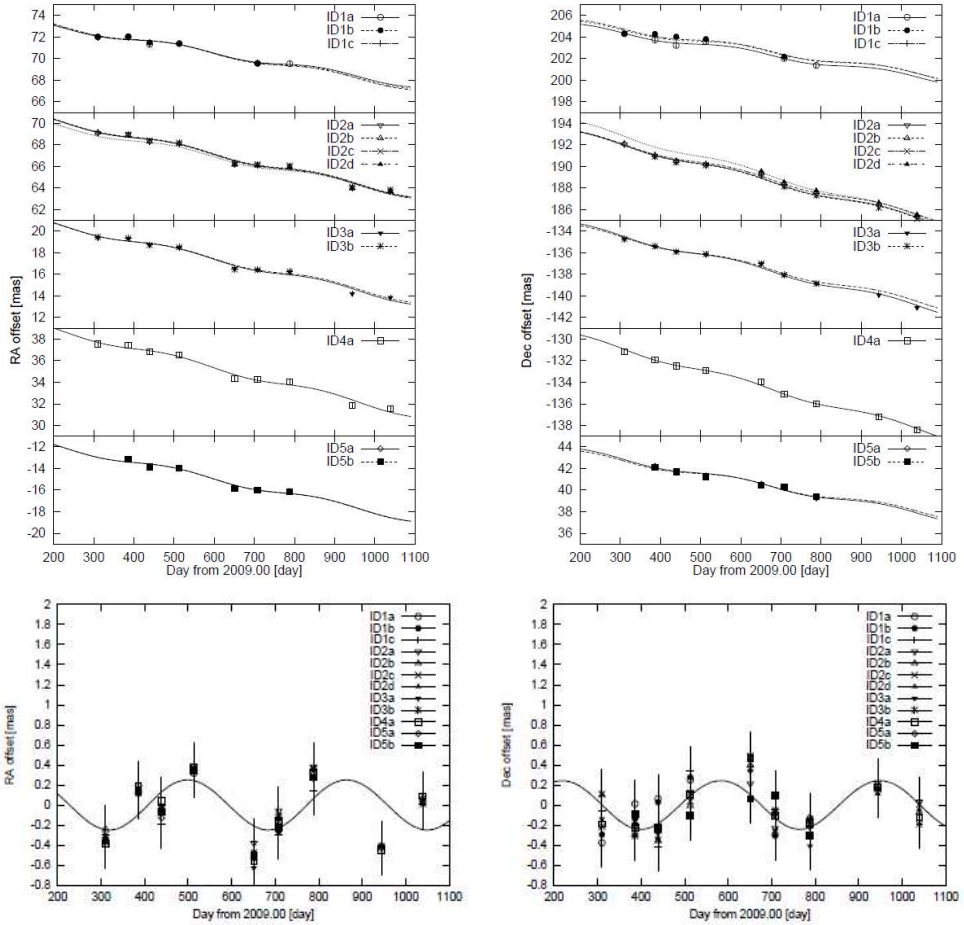

- Annual parallax =0.262±0.031mas 。これは D~3.82kpcに相当
- 固有運動(平均)は、($\mu_\alpha \cos\delta$, μ_δ) = (-2.74, -2.87) mas/yr

Fig. 6

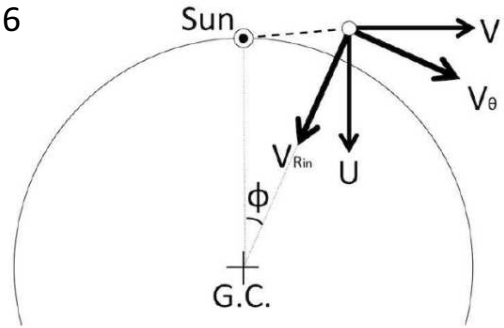

Fig. 6. Schematic depiction definining the velocity vectors (U, V) and $(V_{R_{in}}, V_\theta)$.

観測値とIAU推奨値(R0=8.5kpc, V0=220km/s)より

- R = 9.63kpc
- V_{Rin}= 7.5km/s
- V_θ =202km/s

となる。
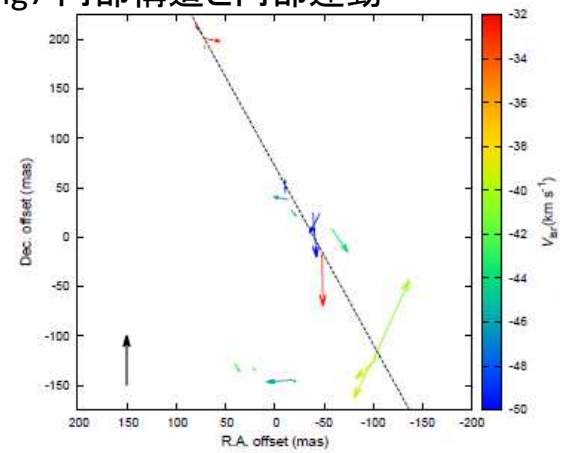
Fig7 内部構造と内部運動